

DC-ViT: Modulating Spatial and Channel Interactions for Multi-Channel Images

Umar Marikkar, Syed Sameed Husain, Muhammad Awais, and Sara Atito

University of Surrey

Abstract. Training and evaluation in multi-channel imaging (MCI) remains challenging due to heterogeneous channel configurations arising from varying staining protocols, sensor types, and acquisition settings. This heterogeneity limits the applicability of fixed-channel encoders commonly used in general computer vision. Recent Multi-Channel Vision Transformers (MC-ViTs) address this by enabling flexible channel inputs, typically by jointly encoding patch tokens from all channels within a unified attention space. However, unrestricted token interactions across channels can lead to feature dilution, reducing the ability to preserve channel-specific semantics that are critical in MCI data. To address this, we propose Decoupled Vision Transformer (DC-ViT), which explicitly regulates information sharing using Decoupled Self-Attention (DSA), which decomposes token updates into two complementary pathways: spatial updates that model intra-channel structure, and channel-wise updates that adaptively integrate cross-channel information. This decoupling mitigates informational collapse while allowing selective inter-channel interaction. To further exploit these enhanced channel-specific representations, we introduce Decoupled Aggregation (DAG), which allows the model to learn task-specific channel importances. Extensive experiments across three MCI benchmarks demonstrate consistent improvements over existing MC-ViT approaches.

Keywords: Multi-Channel Imaging · Vision Transformers

1 Introduction

Training and evaluating vision encoders on Multi-Channel Imaging (MCI) data is fundamentally challenging due to variability in channel configurations across datasets. Unlike natural images, where three RGB channels are standardised, multi-channel images may contain an arbitrary number of channels whose semantics depend on the data acquisition process. This variability arises in diverse settings such as multi-channel microscopy, where different staining protocols produce distinct biological markers, and remote sensing, where sensor modalities and fusion strategies determine spectral composition. For instance, HPA [23] contains four channels, JUMP-CP [6] contains five, WTC-11 [24] contains three, and So2Sat [27] includes 18 channels over multiple spectral bands. This heterogeneity makes it difficult to directly apply fixed-channel encoder designs that are standard in natural image modelling.

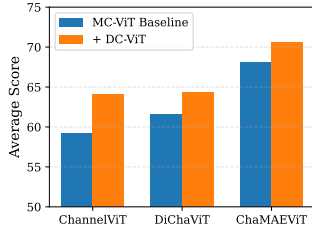


Fig. 1: DC-ViT consistently improves existing MC-ViTs across MCI benchmarks. y-axis is the average score over CHAMMI, JUMP-CP and So2Sat downstream tasks.

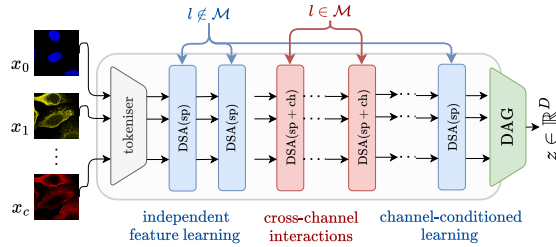


Fig. 2: Schematic of DC-ViT. Channels build strong low-level representations independently, and are then introduced to cross-channel interactions. DSA(sp) and DSA(sp+ch) denote DC-ViT blocks (Eq. (4)) with $l \notin \mathcal{M}$ and $l \in \mathcal{M}$ in Eq. (5), respectively.

To accommodate variable channel configurations, Multi-Channel Vision Transformers (MC-ViT) have emerged as the dominant architecture to train on multi-channel datasets [2, 3, 17, 22]. These models are designed to be channel-adaptive, enabling them to process images with a flexible number of input channels within a unified framework. Following the Vision Transformer (ViT) paradigm [13], each channel is independently partitioned into respective patch tokens, after which all tokens are concatenated into a single sequence and processed jointly by shared self-attention layers. This long sequence formulation allows information to be exchanged freely across spatial locations and channels throughout the encoder architecture.

Under this long-sequence formulation, prior work explores mechanisms to mitigate feature homogenisation across channels. This is achieved either by introducing channel-specific tokens [2, 3], or token diversification losses [22], or a combination of both, and demonstrates that this increased inter-channel diversity generally improves downstream performance. However, despite these modifications, the underlying attention mechanism remains fully shared. Consequently, spatial and channel-wise interactions are entangled, limiting explicit control over how cross-channel information is incorporated.

This unstructured token mixing dilutes channel-specific information within the encoder, thereby limiting the representation capability of MC-ViTs as MCI channels often encode distinct concepts. Yet, complete isolation is also undesirable as certain channels benefit from complementary contextual signals provided by others [14, 19]. The objective is thus not to remove cross-channel interaction, but to regulate it. Motivated by this, we propose Decoupled Vision Transformer (DC-ViT), which explicitly regulates inter-channel interactions within the encoder, while maintaining semantic diversity across channels in the learnt representations. DC-ViT is built upon two components, Decoupled Self-Attention (DSA) and Decoupled Aggregation (DAG), which together regulate inter-channel interaction during encoding and representation aggregation.

To regulate inter-channel interactions, we introduce Decoupled Self-Attention (DSA), which factorises token updates into spatial and a channel-wise components. The spatial branch aggregates information across spatial locations within the same channel to reinforce channel-specific features, while the channel-wise branch adaptively integrates information across channels. This separation enables structured cross-channel interaction and reduces the complexity of fully joint attention. To further leverage channel-specific semantics in forming final representations, we propose Decoupled Aggregation (DAG), a hierarchical aggregation scheme that first produces channel-specific embeddings and then aggregates them to form the final representation. This design explicitly models channel contributions to downstream tasks, aligning the representation structure with the heterogeneous nature of MCI datasets and their task formulations.

Together, DC-ViT provides structured regulation of cross-channel information exchange, mitigating feature dilution while retaining beneficial context sharing. As shown in Fig. 1, across standard MCI benchmarks, DC-ViT consistently outperforms prior MC-ViT baselines.

2 Background and Related Work

Our work is motivated by the observation that channels in MCI datasets carry semantically distinct information which are not effectively encoded in existing MC-ViT architectures. Therefore, we first review evidence of channel heterogeneity across MCI datasets, and then review existing MC-ViT architectures.

Channel Heterogeneity in MCI datasets. The semantic structure of channels in MCI datasets differs fundamentally from that of RGB images, where channels carry largely redundant information. For example, in immunofluorescent (IF) microscopy, individual channels capture a specific aspect of cellular organisation or phenotype. Some channels mainly provide stable structural context, while others encode signals that vary with the biological condition of interest [19]. In the HPA dataset, the protein of interest is imaged together with reference markers for the Nucleus, Microtubules, and Endoplasmic Reticulum, which support the interpretation of protein localisation [23]. In JUMP-CP, DNA and ER channels largely convey positional information, whereas RNA, AGP, and Mitochondrial channels reflect morphology changes induced by perturbations [6, 10]. In WTC-11, the nucleus channel contains the primary biological signal, with membrane and protein channels providing additional context [24]. CM4AI-Bridge2AI adopts a similar staining scheme, combining target proteins with structural markers such as DAPI, anti-tubulin, and ER [9].

Similarly, semantic variation between channels is observed in satellite-based multi-channel imaging. In the So2Sat LCZ42 dataset, channels contain visible, near-infrared, and short-wave infrared bands, each encoding different physical properties of the Earth’s surface [27]. Some bands primarily capture stable geometric or reflectance information, while others are more sensitive to surface materials or human activity. As in IF microscopy, these spectral channels are

not interchangeable, and modelling approaches must account for their distinct roles.

Multi-Channel Vision Transformers. Vision encoders designed for multi-channel imaging (MCI) data have been explored across application domains including climate modelling [16, 20], cell microscopy [8, 12, 14], and satellite imagery [27]. Recent work in this area largely falls under the class of multi-channel Vision Transformers (MC-ViTs), which extend standard Vision Transformers (ViTs) [13] to accommodate MCI data.

Unlike vanilla ViTs, which embed spatial patches from all channels into a single token sequence, MC-ViTs tokenise spatial patches from each channel independently, producing channel-specific token embeddings with spatially aligned positional encodings. This design is first introduced in Climax [20], and later adopted for MCI benchmarks in ChAdaViT [3], which additionally incorporates learnable channel embeddings added to the token representations. Subsequent methods build on ChAdaViT by introducing different training strategies, such as hierarchical channel sampling in ChannelViT [2], diverse token regularisation losses in DiChaViT [22], and masked image modelling [15] as an auxiliary objective in ChaMAEViT [21].

Despite these differences, existing MC-ViTs share a common encoding protocol in which tokens from all channels are concatenated into a single long sequence and processed jointly through self-attention. In contrast, we propose Decoupled Self-Attention, which explicitly separates channel-wise encoding from inter-channel interaction, with the aim of preserving channel-specific representations while enabling efficient and controlled information sharing across channels. Furthermore, existing methods generate final representations via the `cls` token or by global attention pooling over all tokens, both of which fail to take into account the ‘channel importance’ of MCI datasets. We therefore propose Decoupled Aggregation.

3 Methodology

This section presents the proposed Decoupled Vision Transformer (DC-ViT). We first describe the encoding protocol used in existing multi-channel Vision Transformers (MC-ViTs) in Sec. 3.1. We then introduce DC-ViT and detail its architectural components, including Decoupled Self-Attention and hierarchical pooling for multi-channel data Sec. 3.2.

3.1 Preliminaries: The MC-ViT encoding protocol

We describe the encoding protocol of existing MC-ViTs. Let an input MCI image be given as $X \in \mathbb{R}^{C \times H \times W}$, where C denotes the number of channels and H, W are the spatial dimensions.

Unlike traditional ViTs, MC-ViTs apply a shared patch embedding layer independently to each channel, resulting in an input feature representation of

dimensions $C \times N \times D$, where N is the number of tokens per channel and D is the feature dimensionality. Auxiliary token embeddings (i.e.: channel and spatial positional embeddings) are added to this representation afterwards.

Existing MC-ViTs flatten this representation along the channel dimension to yield the token representation $\mathbf{x} \in \mathbb{R}^{CN \times D}$, where CN is the resulting sequence length. In practice, the overall sequence length is $CN + N_{ext}$, where N_{ext} denotes extra tokens (e.g., the `cls` token); for simplicity, we denote the MC-ViT sequence length as CN .

We write the feature update of MC-ViTs as follows, and its schematic can be found in Fig. 3a. At encoder depth l , the next-layer representation is computed using a standard ViT update,

$$\mathbf{x}_{l+1} = \mathbf{x}_l + \text{MLP}(\mathbf{x}_l + \text{MSA}(\mathbf{x}_l)) \in \mathbb{R}^{CN \times D}, \quad (1)$$

where MLP_l is a two-layer feed-forward network with a GELU activation. $\text{MSA}_l(\mathbf{x}_l)$ denotes multi-head self-attention applied over the entire sequence as,

$$\text{MSA}_l(\mathbf{x}_l) = W_O(\text{Attn}(\mathbf{x}_l)) \in \mathbb{R}^{CN \times D}, \quad (2)$$

where W_O is the output projection, and Attn is the computation of scaled dot-product attention, defined as,

$$\text{Attn}(\mathbf{x}_l) = \text{Softmax}\left(\mathbf{q}_l \mathbf{k}_l^\top / \sqrt{D}\right) \mathbf{v}_l, \quad (3)$$

where $\mathbf{q}_l = W_Q(\mathbf{x}_l)$, $\mathbf{k}_l = W_K(\mathbf{x}_l)$, and $\mathbf{v}_l = W_V(\mathbf{x}_l)$ are obtained from linear projections. When applying Eq. (3) in MC-ViTs, the Softmax operation is computed along the full sequence dimension of length CN .

Since attention is performed over the entire CN sequence, there is no explicit constraint on token interactions: any token from any channel and spatial location may aggregate information from all other tokens. We find this to be a limitation of MC-ViTs, as unrestricted interactions can dilute channel-specific representations.

However, completely avoiding inter-channel interactions is also undesirable, as certain channels provide contextual or reference information that aids the interpretation of others [19]. We observe this in preliminary experiments with independently encoded channels (see Tab. 4, $\mathcal{M} = \{\}$), where the absence of cross-channel interactions that yield diverse channel representations in fact leads to lower downstream performance. This indicates that while preserving channel-specific features is important, some level of inter-channel interaction remains necessary for MCI tasks, as channels often provide complementary information to one another.

Therefore, to preserve feature diversity while enabling effective inter-channel interactions, we propose the Decoupled Vision Transformer (DC-ViT), which controls token interactions explicitly through its architectural design. We describe DC-ViT in Sec. 3.2.

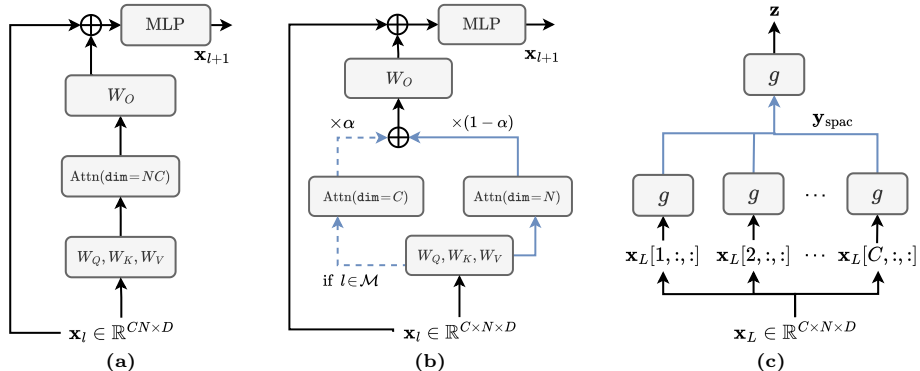


Fig. 3: (a) An MC-ViT layer. Self-attention is performed on a joint set of tokens from all channels. (b) A DC-ViT layer: Self-attention is performed across the set of tokens for a given channel, and across the set of tokens for a given spatial location. Channel attention (dashed path) is only performed when $l \in \mathcal{M}$, in which case α is a learnable scalar. If not, α is fixed to 0. (c) Decoupled Aggregation: Features are aggregated in a hierarchical setting; first spatially and then channel-wise. \rightarrow : tensor reshaping operations.

3.2 Decoupled Vision Transformer (DC-ViT)

Motivated by the observation that channels in MCI datasets encode semantically distinct information, while still being able to benefit from selective inter-channel information sharing, we introduce the Decoupled Vision Transformer (DC-ViT). DC-ViT is designed to preserve rich channel-specific representations while enabling cross-channel interactions beneficial for downstream tasks.

DC-ViT consists of two main components. **Decoupled Self-Attention** decomposes the NC -sequence self-attention into spatial (N) and channel-wise (C) interactions, explicitly separating within-channel and cross-channel token interactions. **Decoupled Aggregation** aggregates features in a hierarchical manner, first within channels and then across channels, rather than from a unified pool of tokens. We describe Decoupled Self-Attention and Decoupled Aggregation in the following subsections.

Decoupled Self-Attention. Let us re-define the input set of patch embeddings as $\mathbf{x} \in \mathbb{R}^{C \times N \times D}$ where C denotes the number of channels, N is the number of tokens per channel, and D is the feature dimensionality. Unlike traditional MC-ViTs, the set of embeddings \mathbf{x} is not flattened to a single channel-sequence dimension (i.e.: $C \times N \rightarrow CN$).

At depth l of an encoder of L layers, a DC-ViT block computes the output representation \mathbf{x}_{l+1} from the input \mathbf{x}_l by decomposing self-attention into channel-wise and spatial components. Queries, keys, and values are obtained through shared linear projections and are used to compute attention independently across channels and across spatial locations. The resulting attention out-

puts are combined using a learnable mixing weight α_l , and the aggregated representation is then passed through shared output projections and an MLP, following the standard ViT design.

Channel attention is only applied at a subset of encoder layers $\mathcal{M} \subseteq \mathcal{L}$, where \mathcal{L} is the set of encoder layer indices, while spatial attention is applied at all layers. This introduces a channel interaction bottleneck in which the encoder first processes channels independently to capture low-level, channel-specific features, then undergoes selective inter-channel information exchange, and finally encodes channel-aware high-level features. This pattern, illustrated in Fig. 2, allows cross-channel dependencies to be learned without compromising channel-specific feature structure.

Formally, given the representation \mathbf{x}_l at encoder depth l , a DC-ViT block computes the next-layer representation as,

$$\mathbf{x}_{l+1} = \mathbf{x}_l + \text{MLP}(\mathbf{x}_l + \text{DSA}(\mathbf{x}_l)) \in \mathbb{R}^{C \times N \times D}. \quad (4)$$

Here, $\text{DSA}(\mathbf{x}_l)$ denotes Decoupled Self-Attention with selective channel interaction, and is defined as,

$$\text{DSA}(\mathbf{x}_l) = \begin{cases} W_O(\alpha \cdot \text{Attn}_{ch}(\mathbf{x}_l) + (1 - \alpha) \cdot \text{Attn}_{sp}(\mathbf{x}_l)), & \text{if } l \in \mathcal{M}, \\ W_O(\text{Attn}_{sp}(\mathbf{x}_l)), & \text{if } l \notin \mathcal{M}, \end{cases} \quad (5)$$

where W_O is the output projection, and α is a learnable scalar for layer $l \in \mathcal{M}$. When $l \notin \mathcal{M}$, channel attention is omitted and the update reduces to a purely spatial attention operation. Unlike the MSA layer in Eq. (2), DSA explicitly separates channel-wise and spatial token interactions, enabling selective modelling of cross-channel dependencies.

Channel attention shares information across channels at a fixed spatial location and is only applied when $l \in \mathcal{M}$. Attn_{ch} is defined as,

$$\text{Attn}_{ch}(\mathbf{x}_l) = [\text{Attn}(\mathbf{x}_{l,n})]_{n=1}^N \in \mathbb{R}^{C \times N \times D}, \quad (6)$$

where $\mathbf{x}_{l,n} \in \mathbb{R}^{C \times D}$ denotes the slice of \mathbf{x}_l at spatial index n . Similarly, spatial attention shares information across the N tokens of a given channel and is applied at all layers. Attn_{sp} is defined as,

$$\text{Attn}_{sp}(\mathbf{x}_l) = [\text{Attn}(\mathbf{x}_{l,c})]_{c=1}^C \in \mathbb{R}^{C \times N \times D}, \quad (7)$$

where $\mathbf{x}_{l,c} \in \mathbb{R}^{N \times D}$ denotes the token sequence for channel c . In both cases, $\text{Attn}(\cdot)$ follows the standard scaled dot-product attention in Eq. (3). The schematic of a DC-ViT layer with selective Decoupled Self-Attention can be found in Fig. 3b.

Decoupled Aggregation. Existing MC-ViTs extract the final representation via the `cls` token or global attention pooling, viewing the set of data tokens as a single unified pool, regardless of the assigned channels. Given that via Decoupled Self-Attention, individual channels may exhibit unique semantic concepts

that may or may not be dependent on other channels, we implement Decoupled Aggregation (DAG). Here, a pooling operation is sequentially applied within-and-across channels, as opposed to pooling from a unified pool of features. We first define a pooling function,

$$g(\cdot) : \mathbb{R}^{N \times D} \mapsto \mathbb{R}^D, \quad (8)$$

which can be any function that reduces the output from a feature map to a single token representation. $g(\cdot)$ may be the extraction of latent tokens such as the `cls` token, mean/max pooling, or an attention-based aggregation function [1, 5, 21].

Given the L 'th layer representation of the encoder $\mathbf{x}_L \in \mathbb{R}^{C \times N \times D}$, Decoupled Aggregation first performs spatial aggregation within each channel, followed by aggregation across channels. First, for each channel c , we apply a spatial pooling function g_{sp} over the N tokens,

$$\mathbf{y}_{spac,c} = g_{sp}(\mathbf{x}_{L,c}), \quad c = 1, \dots, C. \quad (9)$$

Stacking the resulting channel representations yields

$$\mathbf{y}_{spac} = [\mathbf{y}_{spac,c}]_{c=1}^C \in \mathbb{R}^{C \times D}. \quad (10)$$

The final representation is then obtained by aggregating across channels using the channel pooling function g_{ch} ,

$$\mathbf{z} = g_{ch}(\mathbf{y}_{spac}), \quad \mathbf{z} \in \mathbb{R}^D. \quad (11)$$

Together, DSA and DAG provide an encoding protocol that explicitly controls feature interactions across spatial and channel dimensions. This design allows DC-ViT to maintain channel-specific feature diversity while supporting effective inter-channel information exchange for downstream prediction.

4 Experiments

Datasets and Tasks. We conduct experiments on three standard benchmarks widely adopted in prior MC-ViT literature [17, 21, 22]: CHAMMI, JUMP-CP, and So2Sat.

CHAMMI [8] is a microscopy benchmark that contains data from WTC-11 [24], HPA [25], and CP [4]. These sources provide images with varying channel counts (3, 4, and 5 fluorescent channels, respectively). The combined benchmark comprises approximately 220K images in total, including 100K training samples. CHAMMI defines nine downstream evaluation tasks, six of which are designed to assess out-of-distribution (OOD) generalisation. In line with existing MC-ViT works, we report the mean OOD performance on the WTC-11 and HPA subsets.

The JUMP-CP dataset [7] contains multi-channel cellular images acquired under chemical perturbations, with each image consisting of 8 channels (5 fluorescent and 3 bright-field). The dataset is split into 127K training images, 45K validation images, and 45K test images. The downstream task is formulated as a

multi-class classification problem with 161 categories, representing 160 distinct compound perturbations and one control condition.

So2Sat [27] is a remote sensing benchmark constructed from satellite imagery collected by Sentinel-1 and Sentinel-2, providing 8 radar channels and 10 multispectral channels, respectively. The dataset includes 352K training samples, along with 24K samples each for validation and testing. The task is posed as a 17-class classification problem, where each class corresponds to a specific land-cover or surface type, such as vegetation, paved regions, or buildings. For both JUMP-CP and So2Sat, we report results under the full channel count during inference, and partial channel counts during inference, following existing works.

Baseline comparisons. We evaluate DC-ViT under two settings: (i) the standalone performance of DC-ViT as an encoding protocol, and (ii) its generalisation to pre-trained encoders beyond training from scratch.

For architecture comparison, we follow the standard evaluation protocol used in prior MC-ViT studies, where all models are fine-tuned from scratch. To isolate the effect of the encoder architecture, all method-specific training strategies are kept fixed for a fair comparison. For each method, we replace the MC-ViT blocks (Fig. 3a, Eq. (1)) in the encoder backbone of each baseline with the DC-ViT blocks (Fig. 3b, Eq. (4)), and the pooling function with DAG (Fig. 3c, Eq. (11)). For supervised baselines, we compare against ChAdaViT [3], ChannelViT [2], and DiChaViT [22]. For hybrid self-supervised + supervised training, we compare with ChaMAEViT [21]. For ChaMAEViT, to isolate the effect of encoder architecture, we compare against its sampling configuration in which the same spatial locations are sampled across channels. This is due to DC-ViT operating on a one-to-one correspondence between spatial locations across channels for inter-channel attention.

We additionally evaluate the transfer learning performance of DC-ViT when initialised from pre-trained encoders and adapted to downstream MCI tasks. Experiments are conducted on microscopy datasets, where we pre-train two encoders using iBOT [26] on HPAv23 [25] and JUMP-CP [6] single-channel single-cell images, respectively. During pre-training, the encoder learns independent representations for each channel. We perform single-channel pre-training as existing studies show that this transfers effectively to MCI downstream tasks, particularly when the pre-training and fine-tuning channel configurations differ [17, 18]. For fine-tuning, we adopt the same configuration as ChannelViT, using hierarchical channel sampling and latent channel tokens, while replacing the encoder blocks with DC-ViT.

Training and evaluation. Following existing work, we perform our experiments on ViT-S, with patch size 16 for CHAMMI and JUMP-CP, and patch size 8 for So2Sat. Closely following baselines, we set $lr = 4e^{-4}$ for JUMP-CP and So2Sat. For CHAMMI training, we set $lr = 4e^{-4}$ with ChaMAEViT and $lr = 4e^{-5}$ for others. We set the effective batch sizes (over multi-GPU training) as 128 for JUMP-CP and So2Sat, and 64 for CHAMMI. The remaining hyper-parameters

(e.g.: auxiliary loss weights, proxy temperatures) are identical to baselines. In all cases, linear lr scaling is applied where available GPU memory bandwidth is insufficient.

DC-ViT settings. For DSA, we set the channel-attention layer indices from Eq. (6) as $\mathcal{M} = \{4, 6, 8\}$ for all primary experiments, and the effect of different layer indices for \mathcal{M} can be found in Tab. 4. We initialise the scalar channel-interaction weight to $\alpha = 0.1$ across all datasets. Although certain initialisations of α yield stronger metrics, we avoid tuning this parameter to prevent dependence on dataset-specific initialisation. Results for different α initialisations are reported in Tab. 5. For DAG, We set g_{sp} to be an ABMIL aggregator, which dynamically assigns a scalar weighting for each feature [5]. Channel pooling function g_{ch} is set as the max-pooling operator, over the channel (C) dimension. We compare different choices for g_{sp} and g_{ch} in Tab. 6.

For additional results in Tab. 3, Tab. 4, Tab. 5, and Tab. 6, unless stated otherwise, we fix $\mathcal{M} = \{4, 6, 8\}$, set $\alpha = 0.1$, use ABMIL for both g_{sp} and g_{ch} . These values are the default configuration, except for the parameters explicitly varied for analysis.

5 Results

5.1 MCI benchmarks

We evaluate our method in two settings: (1) fine-tuning from scratch compared to existing MC-ViTs, and (2) fine-tuning from pre-trained checkpoints to assess the transfer learning capability of DC-ViT.

Architecture comparison. Tab. 1 reports downstream performance on MCI benchmarks compared to existing MC-ViTs. DC-ViT shows consistent improvements across nearly all metrics, including when self-supervision is used as an auxiliary objective (e.g., ChaMAEViT). However, we observe a degradation for ChAdaViT under partial-channel evaluation. Since ChAdaViT is trained without channel sampling, its performance already degrades when channels are missing. In our case, this effect is amplified because channel attention in DSA must compute the softmax over fewer channels than seen during training. Nevertheless, since channel sampling is employed in all succeeding methods, this issue is largely mitigated, and DC-ViT still achieves substantial improvements overall.

Generalisation to pre-trained models. Tab. 2 reports transfer learning performance on MCI benchmarks using different pre-trained encoder checkpoints under the ChannelViT training pipeline. DC-ViT consistently improves over vanilla ChannelViT under both pre-trained models, consistent with the gains observed when training from scratch. This indicates that DC-ViT transfers more effectively from pre-trained encoders than existing MC-ViTs. We attribute this to the fact that commonly used pre-trained models for MCI are largely channel-agnostic, as they are trained on single-channel inputs [17]. Introducing restricted

Table 1: Performance on MCI benchmarks w.r.t encoder architecture. All methods are trained from scratch.

| Method | DC-ViT | CHAMMI | JUMP-CP | | So2Sat | |
|------------|--------|--------|---------|---------|--------|---------|
| | | Avg. | Full | Partial | Full | Partial |
| ChAdaViT | ✗ | 63.88 | 65.03 | 42.15 | 56.98 | 12.38 |
| | ✓ | 68.91 | 69.53 | 25.09 | 62.56 | 10.63 |
| ChannelViT | ✗ | 64.90 | 67.51 | 56.49 | 61.03 | 46.16 |
| | ✓ | 71.72 | 73.26 | 61.90 | 64.97 | 48.61 |
| DiChaViT | ✗ | 69.68 | 69.19 | 57.98 | 63.36 | 47.76 |
| | ✓ | 72.04 | 73.20 | 62.34 | 65.99 | 48.25 |
| ChaMAEViT | ✗ | 73.13 | 85.23 | 66.85 | 65.14 | 50.01 |
| | ✓ | 76.33 | 86.11 | 70.02 | 67.57 | 53.11 |

Table 2: Transfer learning comparison on microscopy benchmarks. We adopt the ChannelViT training pipeline.

| | DC-ViT | CHAMMI | JUMP-CP | |
|---------|--------|--------|---------|---------|
| | | Avg. | Full | Partial |
| Scratch | ✗ | 64.90 | 67.51 | 56.49 |
| | ✓ | 71.72 | 73.26 | 61.90 |
| HPA | ✗ | 70.22 | 82.24 | 67.55 |
| | ✓ | 77.15 | 83.08 | 68.77 |
| JUMP | ✗ | 70.01 | 75.84 | 62.95 |
| | ✓ | 73.29 | 78.72 | 65.20 |

Table 3: Ablation of DSA and DAG. Absence of both components is equivalent to ChannelViT with attention pooling.

| Components | | CHAMMI | JUMP-CP | |
|------------|-----|--------|---------|---------|
| DSA | DAG | Avg. | Full | Partial |
| ✓ | ✓ | 71.72 | 73.26 | 61.90 |
| ✓ | ✗ | 70.02 | 70.70 | 62.41 |
| ✗ | ✓ | 63.46 | 67.03 | 56.42 |
| ✗ | ✗ | 62.91 | 66.15 | 57.20 |

inter-channel interactions during fine-tuning enables the model to incorporate cross-channel information while maintaining compatibility with the representations learnt during single-channel pre-training.

5.2 Analysis

We analyse the contribution of each component and the sensitivity to its configuration. Specifically, we first examine the contribution of DSA and DAG through component ablation, and also discuss the computational efficiency of DC-ViT vs. the existing MC-ViT encoding protocol. We then study the sensitivity to the initialisation of α and the placement of inter-channel interaction blocks ($l \in \mathcal{M}$) within the encoder. Finally, we evaluate the generalisability to alternative pooling functions within the DAG hierarchical framework.

Contribution of DSA and DAG. We ablate the two main components of DC-ViT, Decoupled Self-Attention (DSA) and Decoupled Aggregation (DAG).

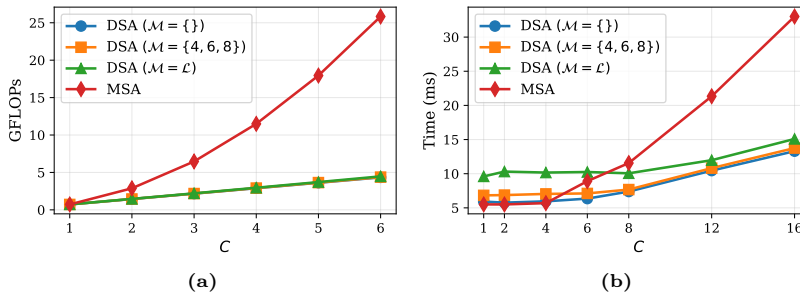


Fig. 4: (a) The calculated number of FLOPs for the attention computation (i.e.: query-key matrix multiplication, softmax calculation, and attention-value matrix multiplication) for DSA in DC-ViT vs. traditional NC sequence MSA in MC-ViTs. We observe a linear increase in FLOPs for DSA vs. an exponential increase in FLOPs for MSA, per channel count. (b) Time taken for a single forward pass per sample of DC-ViT vs. MC-ViT encoder. For higher channel counts, DSA is much more efficient.

We first replace DSA with joint self-attention in MC-ViTs. Under this setting, DAG is carried out by splitting feature tokens of individual channels (i.e.: $NC \rightarrow N \times C$). Secondly, we keep DSA, but replace DAG with joint pooling of all features (i.e.: pooling directly from NC tokens) using the same pooling function. We finally ablate both components, which is equivalent to an MC-ViT (ChannelViT) with attention pooling as opposed to extracting the `cls` token.

From Tab. 3, we observe that removing either DSA or DAG from the baseline configuration degrades downstream performance, with a larger drop observed when ablating DSA. When both components are removed, performance deteriorates substantially and is similar to ChannelViT, indicating that both components are necessary for strong performance.

Computational complexity. We evaluate computational complexity using two measures: (i) theoretical FLOPs of the attention component and (ii) runtime measured as the time for a single forward pass, across varying channel counts. We also consider different levels of inter-channel interaction: (1) $\mathcal{M} = \{\}$, where attention operates only within channels; (2) $\mathcal{M} = \{4, 6, 8\}$, where three layers contain inter-channel interactions; and (3) $\mathcal{M} = \mathcal{L}$, where all layers include inter-channel interactions.

For FLOP computation, we consider only the query-key multiplication, softmax, and attention-value multiplication, since projection layers and MLPs are identical between DSA and MSA. Fig. 4a shows the resulting FLOPs across channel counts. MSA scales quadratically with channels, whereas DSA increases near-linearly, following $O(C^2N^2)$ for MSA and $O(CN^2 + NC^2)$ for DSA. With $C \ll N$, the NC^2 term becomes negligible.

From Fig. 4b, DSA shows a small runtime overhead at low channel counts but remains stable as C increases, unlike MSA which grows rapidly. We find an additional overhead introduced with increasing $|\mathcal{M}|$ since layers with chan-

Table 4: Effect of channel attention layer indices \mathcal{M} . $\{1\}$ and $\{12\}$ denote the first and final layers of the 12-layer encoder, respectively, and $\mathcal{L} = \{1, \dots, 12\}$ denotes the set of all layers. The top-3 values are highlighted.

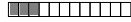
| Layers (\mathcal{M}) | CHAMMI | | | JUMP-CP | | |
|---|--------|-------|---------|---------|---------|--|
| | Avg. | Full | Partial | Full | Partial | |
| $\{\}$ (none)  | 66.15 | 47.72 | 44.65 | | | |
| $\{1,2,3\}$  | 70.88 | 67.52 | 58.90 | | | |
| $\{1,3,5\}$  | 71.23 | 69.13 | 59.45 | | | |
| $\{5,6,7\}$  | 72.56 | 69.54 | 59.48 | | | |
| $\{4,6,8\}$  | 71.57 | 71.28 | 61.13 | | | |
| $\{8,10,12\}$  | 70.46 | 69.69 | 60.04 | | | |
| $\{10,11,12\}$  | 72.80 | 69.08 | 59.18 | | | |
| \mathcal{L} (all)  | 69.49 | 71.36 | 60.92 | | | |

Table 5: Effect of α value.

| α | CHAMMI | JUMP-CP | | So2Sat | |
|----------|--------|---------|---------|--------|---------|
| | Avg. | Full | Partial | Full | Partial |
| 0.00 | 72.09 | 71.80 | 61.23 | 65.16 | 48.46 |
| 0.10 | 71.57 | 71.28 | 61.13 | 65.76 | 48.41 |
| 0.25 | 71.46 | 72.52 | 61.37 | 65.10 | 49.05 |
| 0.50 | 69.27 | 71.64 | 61.45 | 65.51 | 49.14 |

Table 6: Effect of pooling function.

| $g_{sp} g_{ch}$ | CHAMMI | | | JUMP-CP | | |
|-----------------|--------|-------|---------|---------|---------|--|
| | Avg. | Full | Partial | Full | Partial | |
| cls | mean | 66.96 | 72.46 | 60.90 | | |
| | max | 71.14 | 72.34 | 61.35 | | |
| | abmil | 72.09 | 71.56 | 61.44 | | |
| abmil | mean | 65.43 | 73.01 | 61.52 | | |
| | max | 71.72 | 73.26 | 61.90 | | |
| | abmil | 71.57 | 71.28 | 61.13 | | |

nel interaction call the attention kernel twice. As FlashAttention [11] is used by default, these calls are not parallelised and is therefore slow. We therefore implement channel-attention using the `math` kernel, though a small runtime buffer still remains. Nevertheless, for larger channel counts, DSA is significantly faster.

Choice of Channel Attention Layers \mathcal{M} . Beyond the regularisation induced by restricting information flow in DC-ViT, selecting a subset of layers $\mathcal{M} \subseteq \mathcal{L}$ (where \mathcal{L} denotes the full set of encoder layers) at which channel attention is applied introduces an additional structural bottleneck. This bottleneck encourages earlier layers to build strong individual channel representations, and reduces computational cost, as shown in Fig. 4.

To study the effect of channel attention placement, we evaluate multiple configurations by varying the location of \mathcal{M} within the encoder while fixing $|\mathcal{M}| = 3$. Results are reported in Tab. 4, where we observe that applying channel attention in the early layers leads to reduced performance, while deferring it to later layers improves results. Performance also decreases when channel attention is applied only in the final layers. This is due to the pooling algorithm DAG favouring diverse features as input, as enabling inter-channel interaction in the latter layers increases mutual information between channels. Hence, the best performance is obtained when inter-channel interactions are induced in the middle layers of the backbone (e.g., $\mathcal{M} = \{4, 6, 8\}$).

These results indicate that early layers benefit from independent low-level feature extraction. The information sharing in the intermediate layers generates channel-conditioned representations, where each channel is enhanced via auxiliary information from other channels. Therefore, we restrict \mathcal{M} to the middle

layers to retain informative channel interactions while avoiding unnecessary computation elsewhere.

Initialisation of α . We study the effect of the initialisation of α in Tab. 5. On benchmarks such as CHAMMI, whose downstream tasks rely more heavily on standalone channels, lower initialisation values of α lead to better performance, suggesting that preserving independent channel representations is more beneficial than inducing inter-channel interactions.

However, since α is learnable, it adapts during training according to the task. For instance, when initialised at 0.1 across all datasets, the final average values (over the set of \mathcal{M} layers) converge to $\alpha = 0.107$ for CHAMMI, $\alpha = 0.411$ for JUMP-CP, and $\alpha = 0.694$ for So2Sat. The initialisation therefore acts mainly as a bias that steers α towards a preferred range and does not require strict dataset-specific tuning. Nevertheless, by initialising α closer to near-optimal values per dataset, given that per-dataset parameter tuning is common practice in existing MC-ViT studies [21, 22], better performance can be achieved.

Dependence on pooling function. From Tab. 6, we observe that performance remains strong as long as channel importance is learned during the final aggregation stage, on datasets where channel importance is more relevant. This is evident when the `mean` operator is used as the channel aggregator for CHAMMI, where the metrics drop substantially. Using attention-based pooling instead of extracting the per-channel `cls` token yields slightly better results in some cases, but the improvement is not significant. Overall, the key remains adhering to the decoupled aggregation scheme.

6 Conclusion

In this work, we address the challenge of learning effective representations from MCI data, where heterogeneous channel configurations and distinct channel semantics make conventional fixed-channel encoders unsuitable. We introduce Decoupled Vision Transformer (DC-ViT), a framework that explicitly regulates cross-channel information exchange through Decoupled Self-Attention (DSA), and leverages learnt representations effectively for downstream tasks through Decoupled Aggregation (DAG). By separating spatial and channel-wise interactions during encoding and hierarchically aggregating channel representations, DC-ViT preserves channel-specific semantics while enabling beneficial contextual information sharing. Extensive experiments across multiple MCI benchmarks show that incorporating DC-ViT consistently improves the performance of existing MC-ViT architectures. These results indicate that explicitly structuring inter-channel interactions is critical for effectively modelling the heterogeneous and semantically diverse nature of MCI data. Overall, DC-ViT provides a simple yet effective architectural modification that better captures the inherent characteristics of multi-channel imaging datasets, leading to more robust and informative representations for downstream tasks.

References

1. Assran, M., Bardes, A., Fan, D., Garrido, Q., Howes, R., Muckley, M., Rizvi, A., Roberts, C., Sinha, K., Zhulus, A., et al.: V-jepa 2: Self-supervised video models enable understanding, prediction and planning. arXiv preprint arXiv:2506.09985 (2025) 8
2. Bao, Y., Sivanandan, S., Karaletsos, T.: Channel vision transformers: An image is worth 1 x 16 x 16 words. In: The Twelfth International Conference on Learning Representations (2024) 2, 4, 9, 17
3. Bourriez, N., Bendidi, I., Cohen, E., Watkinson, G., Sanchez, M., Bollot, G., Genovesio, A.: Chada-vit: Channel adaptive attention for joint representation learning of heterogeneous microscopy images. In: Proceedings of the IEEE/CVF Conference on Computer Vision and Pattern Recognition. pp. 11556–11565 (2024) 2, 4, 9, 17
4. Bray, M.A., Singh, S., Han, H., Davis, C.T., Borgeson, B., Hartland, C., Kost-Alimova, M., Gustafsdottir, S.M., Gibson, C.C., Carpenter, A.E.: Cell painting, a high-content image-based assay for morphological profiling using multiplexed fluorescent dyes. *Nature protocols* **11**(9), 1757–1774 (2016) 8
5. Carbonneau, M.A., Cheplygina, V., Granger, E., Gagnon, G.: Multiple instance learning: A survey of problem characteristics and applications. *Pattern recognition* **77**, 329–353 (2018) 8, 10
6. Chandrasekaran, S.N., Ackerman, J., Alix, E., Ando, D.M., Arevalo, J., Bennion, M., Boisseau, N., Borowa, A., Boyd, J.D., Brino, L., et al.: Jump cell painting dataset: morphological impact of 136,000 chemical and genetic perturbations. *BioRxiv* pp. 2023–03 (2023) 1, 3, 9
7. Chandrasekaran, S.N., Cimini, B.A., Goodale, A., Miller, L., Kost-Alimova, M., Jamali, N., Doench, J.G., Fritchman, B., Skepner, A., Melanson, M., et al.: Three million images and morphological profiles of cells treated with matched chemical and genetic perturbations. *Nature Methods* **21**(6), 1114–1121 (2024) 8
8. Chen, Z.S., Pham, C., Wang, S., Doron, M., Moshkov, N., Plummer, B., Caicedo, J.C.: Chammi: A benchmark for channel-adaptive models in microscopy imaging. *Advances in Neural Information Processing Systems* **36**, 19700–19713 (2023) 4, 8
9. Clark, T., Mohan, J., Schaffer, L., Obernier, K., Al Manir, S., Churas, C.P., Dailamy, A., Doctor, Y., Forget, A., Hansen, J.N., et al.: Cell maps for artificial intelligence: Ai-ready maps of human cell architecture from disease-relevant cell lines. *bioRxiv* (2024) 3
10. von Coburg, E., Wedler, M., Muino, J.M., Wolff, C., Körber, N., Dunst, S., Liu, S.: Cell painting plus: expanding the multiplexing capacity of cell painting-based phenotypic profiling using iterative staining-elution cycles. *Nature Communications* **16**(1), 3857 (2025) 3
11. Dao, T., Fu, D., Ermon, S., Rudra, A., Ré, C.: Flashattention: Fast and memory-efficient exact attention with io-awareness. *Advances in neural information processing systems* **35**, 16344–16359 (2022) 13
12. Doron, M., Moutakanni, T., Chen, Z.S., Moshkov, N., Caron, M., Touvron, H., Bojanowski, P., Pernice, W.M., Caicedo, J.C.: Unbiased single-cell morphology with self-supervised vision transformers. *bioRxiv* (2023) 4
13. Dosovitskiy, A., Beyer, L., Kolesnikov, A., Weissenborn, D., Zhai, X., Unterthiner, T., Dehghani, M., Minderer, M., Heigold, G., Gelly, S., Uszkoreit, J., Houlsby, N.: An image is worth 16x16 words: Transformers for image recognition at scale. In: *International Conference on Learning Representations* (2021) 2, 4

14. Gupta, A., Wefers, Z., Kahnert, K., Hansen, J.N., Leineweber, W., Cesnik, A., Lu, D., Axelsson, U., Ballllosera Navarro, F., Karaletsos, T., et al.: Subcell: Vision foundation models for microscopy capture single-cell biology. *bioRxiv* pp. 2024–12 (2024) 2, 4
15. He, K., Chen, X., Xie, S., Li, Y., Dollár, P., Girshick, R.: Masked autoencoders are scalable vision learners. In: *Proceedings of the IEEE/CVF conference on computer vision and pattern recognition*. pp. 16000–16009 (2022) 4
16. Herruzo, P., Gruca, A., Lliso, L., Calbet, X., Rípodas, P., Hochreiter, S., Kopp, M., Kreil, D.P.: High-resolution multi-channel weather forecasting – first insights on transfer learning from the weather4cast competitions 2021. In: *2021 IEEE International Conference on Big Data (Big Data)*. pp. 5750–5757 (2021) 4
17. Lian, W., Lindblad, J., Micke, P., Sladoje, N.: Isolated channel vision transformers: From single-channel pretraining to multi-channel finetuning. *arXiv preprint arXiv:2503.09826* (2025) 2, 8, 9, 10
18. Lorenci, A.V.D., Yi, S.E., Moutakanni, T., Bojanowski, P., camille couprie, Caicedo, J.C., Pernice, W.M.A.: Scaling channel-invariant self-supervised learning (2025) 9
19. Marikkar, U., Husain, S.S., Awais, M., Atito, S.: C3r: Channel conditioned cell representations for unified evaluation in microscopy imaging. *arXiv preprint arXiv:2505.18745* (2025) 2, 3, 5
20. Nguyen, T., Brandstetter, J., Kapoor, A., Gupta, J.K., Grover, A.: Climax: A foundation model for weather and climate. *arXiv preprint arXiv:2301.10343* (2023) 4
21. Pham, C., Caicedo, J.C., Plummer, B.A.: Cha-maevit: Unifying channel-aware masked autoencoders and multi-channel vision transformers for improved cross-channel learning. In: *Advances in Neural Information Processing Systems (NeurIPS)* (2025) 4, 8, 9, 14, 17, 19
22. Pham, C., Plummer, B.: Enhancing feature diversity boosts channel-adaptive vision transformers. *Advances in Neural Information Processing Systems* **37**, 89782–89805 (2024) 2, 4, 8, 9, 14, 17
23. Thul, P.J., Åkesson, L., Wiking, M., Mahdessian, D., Geladaki, A., Ait Blal, H., Alm, T., Asplund, A., Björk, L., Breckels, L.M., et al.: A subcellular map of the human proteome. *Science* **356**(6340), eaal3321 (2017) 1, 3
24. Viana, M.P., Chen, J., Knijnenburg, T.A., Vasan, R., Yan, C., Arakaki, J.E., Bailey, M., Berry, B., Borensztein, A., Brown, E.M., et al.: Integrated intracellular organization and its variations in human ips cells. *Nature* **613**(7943), 345–354 (2023) 1, 3, 8
25. Winsnes, C., Lundberg, E., Maggie, Culliton, P., Le, T., UAxelsson, Ouyang, W.: Human protein atlas - single cell classification. <https://kaggle.com/competitions/hpa-single-cell-image-classification> (2021), kaggle 8, 9
26. Zhou, J., Wei, C., Wang, H., Shen, W., Xie, C., Yuille, A., Kong, T.: ibot: Image bert pre-training with online tokenizer. *arXiv preprint arXiv:2111.07832* (2021) 9
27. Zhu, X.X., Hu, J., Qiu, C., Shi, Y., Kang, J., Mou, L., Bagheri, H., Häberle, M., Hua, Y., Huang, R., Hughes, L., Li, H., Sun, Y., Zhang, G., Han, S., Schmitt, M., Wang, Y.: So2sat lcz42: A benchmark dataset for global local climate zones classification (2019), <https://arxiv.org/abs/1912.12171> 1, 3, 4, 9

Appendices

Overview

In this appendix, we first provide the required implementation details needed to reproduce our work. We also provide access to the model and training code within the supplementary material. We then provide additional results which supplement the original results in the main paper.

A Further implementation details

A.1 Hyperparameter settings

We use the reported values in existing work for all baseline comparisons [21,22]. For training, except for the learning rate, we faithfully follow the recommended hyper-parameter settings in existing works [21,22]. This means, whenever DC-ViT is applied to an existing method, the hyper-parameters of that training setting remain the same as the comparative study, with learning rate adjustments made to validation sets. However, unlike previous works, we perform training with automatic mixed-precision set to FP16 to reduce training time.

For comparisons against fully supervised baselines (ChAdaViT [3], ChannelViT [2], DiChaViT [22]), we train the models for 60 epochs on CHAMMI, and 100 epochs on JUMP-CP and So2Sat. For CHAMMI training and evaluation, we use the DiChaViT codebase¹, and for JUMP-CP and So2Sat, we use the ChaMAEViT codebase² with the settings [mae_loss=0, cross_entropy_loss=1, decoder=None, depth=12, training_sample=None (ChaAdaViT), hcs (ChannelViT), dcs (DiChaViT)].

For comparisons against the supervised + self-supervised hybrid ChaMAEViT [21], we train all models for 100 epochs, and use their codebase for training. However, instead of dynamic patch masking, we perform shared per-channel patch masking where the masking indices are shared throughout the set of sampled channels.

The learnable scalar weighting α is initialised as an nn.Parameter per layer l where $l \in \mathcal{M}$. For CHAMMI, as training data consists of 3 datasets and these datasets may benefit from different degrees of inter-channel information sharing, we set 3 scalar parameters per layer. We find that this leads to marginally better metrics on CHAMMI evaluation, but a single parameter per layer is sufficient as it still outperforms baselines. Further, a single parameter is simpler to implement as it is dataset agnostic.

A.2 DSA pseudo-code

The Decoupled Self-Attention (DSA) in Listing 1.1, computes attention independently across two spaces using shared query, key, and value projections. Spatial

¹ https://github.com/chaudatascience/diverse_channel_vit

² https://github.com/chaudatascience/cha_mae_vit

attention is applied by rearranging the input to treat each channel independently, computing token-to-token interactions across the N patch tokens per channel. For layers $l \in \mathcal{M}$, channel attention is additionally computed by rearranging the input to treat each token independently, capturing channel-to-channel interactions across C channels. The outputs of the two attention computations are then combined via a learnable scalar α , and added residually to the input. For all other layers where $l \notin \mathcal{M}$, only spatial attention is applied.

Listing 1.1: Pytorch pseudo-code for Decoupled Self-Attention (DSA). `F.sdpa` denotes the scaled dot-product attention function in pytorch. Heads are omitted for simplicity.

```
class DSA(nn.Module):
    def __init__(self, dim, channel_attn=True, chan_alpha=0.0):
        self.w_q = nn.Linear(dim, dim)
        self.w_k = nn.Linear(dim, dim)
        self.w_v = nn.Linear(dim, dim)
        self.w_o = nn.Linear(dim, dim)
        if channel_attn: # 1 in M
            self.alpha = nn.Parameter(torch.tensor(chan_alpha))

    def forward(self, x): # x: Tensor[B, C, N, D]
        Q, K, V = self.w_q(x), self.w_k(x), self.w_v(x)

        with sdpa_kernel(FlashAttention):
            A_sp = F.sdpa(rearrange(Q,K,V,'b c n d -> (b c) n d'))
            A_sp = rearrange(A_sp, '(b c) n d -> b c n d')

        if channel_attn: # 1 in M

            with sdpa_kernel(Math): # channel
                A_ch = F.sdpa(rearrange(Q,K,V,'b c n d -> (b n) c d'))
                A_ch = rearrange(A_ch, '(b n) c d -> b c n d')
                A = self.alpha * A_ch + (1 - self.alpha) * A_sp

        else:
            A = A_sp

        return x + self.w_o(A)
```

B Additional results

B.1 Comparison vs. ChaMAEViT under random patch sampling

Tab. 7 shows the comparison vs. ChaMAEViT with dynamic patch sampling, where a random independent set of patches are sampled per channel. We observe that while random patch sampling performs better than shared patch sampling for ChaMAEViT without DC-ViT, using DC-ViT with shared patch sampling outperforms the best ChaMAEViT setting on 4/5 metrics. However, this brings us to a limitation of DC-ViT where inter-channel interactions require a 1-1 correspondence between tokens of individual channels, making random sampling unfeasible with DC-ViT. We aim to address this via methods such as nearest-neighbour or optimal transport alignment to build patch correspondences for inter-channel interactions in future work.

Table 7: Comparison between ChaMAEViT random and shared patch sampling.

| DC-ViT | Sampling | CHAMMI | JUMP-CP | | So2Sat | |
|--------|----------|--------|---------|---------|--------|---------|
| | | Avg. | Full | Partial | Full | Partial |
| ✗ | Shared | 73.13 | 85.23 | 66.85 | 65.14 | 50.01 |
| | Random | 74.63 | 90.73 | 68.05 | 67.44 | 52.11 |
| ✓ | Shared | 76.33 | 86.11 | 70.02 | 67.57 | 53.11 |

B.2 Full results on CHAMMI

Tab. 8 reports the per-task F1 scores on the CHAMMI benchmark. DC-ViT consistently improves performance across most tasks and methods, with gains observed in the majority of WTC, HPA, and CP dataset tasks, demonstrating the effectiveness of the DC-ViT backbone as a drop-in improvement over standard MC-ViT architectures.

Table 8: F1 Scores of MC-ViT models vs. DC-ViT on CHAMMI benchmark. “OOD” refers to out-of-distribution tasks. Baseline values are obtained from ChaMAEViT [21].

| Method | DC-ViT | Average OOD | | | | WTC | | HPA | | | CP | | | |
|-------------|--------|-------------|-------|-------|-------|-------|-------|-------|-------|-------|-------|-------|-------|-------|
| | | Mean | WTC | HPA | CP | Task1 | Task2 | Task1 | Task2 | Task3 | Task1 | Task2 | Task3 | Task4 |
| ChAda-ViT | ✗ | 50.82 | 67.18 | 60.67 | 24.60 | 77.58 | 67.18 | 87.49 | 75.94 | 45.41 | 83.92 | 45.58 | 21.94 | 6.28 |
| | ✓ | 56.05 | 72.06 | 67.76 | 28.32 | 78.01 | 72.06 | 93.54 | 88.42 | 47.09 | 86.09 | 56.22 | 22.61 | 6.14 |
| Channel-ViT | ✗ | 52.54 | 67.58 | 62.35 | 27.81 | 78.36 | 67.58 | 83.93 | 76.73 | 47.97 | 77.70 | 55.16 | 21.89 | 6.38 |
| | ✓ | 56.93 | 73.04 | 70.40 | 27.35 | 82.00 | 73.04 | 92.01 | 87.92 | 52.87 | 85.95 | 54.31 | 22.28 | 5.45 |
| DiCha-ViT | ✗ | 55.36 | 75.18 | 64.36 | 26.53 | 80.87 | 75.18 | 88.08 | 79.26 | 49.45 | 84.08 | 53.03 | 20.95 | 5.60 |
| | ✓ | 56.82 | 75.47 | 68.60 | 26.39 | 80.06 | 75.47 | 90.73 | 87.31 | 49.90 | 81.15 | 52.06 | 21.56 | 5.54 |
| ChAMAE-ViT | ✗ | 58.02 | 77.15 | 72.11 | 24.81 | 84.52 | 77.15 | 94.14 | 87.47 | 56.75 | 90.89 | 56.68 | 10.25 | 7.50 |
| | ✓ | 58.54 | 80.38 | 72.37 | 22.87 | 86.29 | 80.38 | 96.25 | 92.46 | 52.28 | 95.38 | 47.65 | 10.10 | 10.86 |